Supporting Information

Santoso et al. 10.1073/pnas.0910909107

SI Text

SI Materials and Methods. *DNA.* DNA oligonucleotides were synthesized by the Keck Biotechnology Resource Laboratory at Yale Medical School and were purified by denaturing polyacrylamide gel electrophoresis as described previously (1). Most of the experiments in this study used the hairpin DNA shown in Fig. 1C. DNA molecules of this type bind to wild-type Pol I(KF) with a $K_d < 1$ nM (2).

Cysteine substitutions in Pol I(KF). Pol I(KF) derivatives carrying the substitutions L744C and K550C, singly and in combination, were purified from a Pol I(KF) expression construct having the genotype N-His$_6$,D424A,C907S, as described previously (3, 4). (For simplicity, the proteins in this study are described simply by their cysteine substitutions or fluorophore modifications.) The changes listed above all had a negligible effect on polymerase activity (Fig. S2).

Protein labeling. Labeling of Pol I(KF) mutants with sulfhydryl-specific fluorophores was based on the manufacturers' recommendations and our own published procedures (4). Before labeling, the Cys-containing Pol I(KF) derivatives were reduced in the presence of 10 mM DTT and dialyzed into the nonsulfhydryl reducing agent, TCEP (Invitrogen). The single-Cys K550C or L744C proteins were labeled with a 2-fold molar excess of the maleimide derivative of Cy3B (GE Healthcare) or ATTO647N (ATTO-TEC) for 30 min at 22 °C followed by 4.5 h at 4 °C. Under these same conditions, a Pol I(KF) derivative lacking Cys side chains did not become labeled. The double-Cys K550C,L744C protein was labeled by sequential addition of the two maleimides; the slightly greater reactivity of Cys-550 resulted in this side chain being derivatized predominantly by the first reagent to be added (the bias in favor of Cys-550 was 8.3-fold for Cy3B and 2.3-fold for ATTO647N). The first maleimide was equimolar with the protein and was allowed to react for 1 h at 22 °C; the second maleimide was then added at 3-fold molar excess and incubated for a further 16 h at 4 °C. The reaction was stopped by addition of DTT to 1 mM, and the unincorporated fluorophores were removed by gel filtration on a Bio-Spin 30 column. Labeled proteins were stored at −20 °C in 50 mM Tris-HCl, pH 7.5, 1 mM DTT, 40% (vol/vol) glycerol. The extent of labeling, calculated from the UV spectrum, was typically ≥70%.

Ensemble fluorescence spectroscopy. Fluorescence emission spectra were recorded at 22 °C on a Photon Technology International scanning spectrofluorometer. Steady-state fluorescence anisotropy was measured using Glan-Thompson polarizers, with G-factor corrections. Specific experiments are described in the legends to Fig. S1 and Fig. S8.

Analysis of doubly labeled Pol I(KF). The relative amounts of Cy3B and ATTO647N at Pol I(KF) positions 550 and 744 were determined using partial digestion with chymotrypsin (Sigma-Aldrich, protein sequencing grade). Labeled Pol I(KF) (≈3 μM) in 100 mM Tris.HCl, pH 8.0, 10 mM CaCl$_2$, 1 mg/ml bovine serum albumin (BSA), 0.1% (wt/vol) SDS was digested with 4 μg/ml chymotrypsin for 40 s at 22 °C. The reaction was stopped by addition of 2.5 vol of 2 mM phenylmethylsulfonyl fluoride in 25 mM EDTA, pH 8.0, 2% (wt/vol) SDS. Samples were analyzed by SDS-PAGE on a 10% gel, with singly labeled K550C or L744C Pol I(KF) as markers, and were quantitated as described in the legend to Fig. S1.

Pol I(KF) kinetics. The enzymatic activity of Pol I(KF) derivatives was assessed by measuring the rate of nucleotide addition to a DNA primer terminus by chemical quench methods (4, 5). To rule out the possibility that the chemical quench assays might be measuring the reaction rate of a subpopulation of unlabeled polymerase, we also used stopped-flow fluorescence, analogous to methods described previously (4), to obtain rate information (for fingers-closing and for the rate-limiting step of chemical incorporation) derived exclusively from the labeled molecules in a mixture (Fig. S2).

Single-molecule confocal experiments. Doubly labeled Pol I(KF) was present at ≈100 pM in single-molecule observation buffer [40 mM Hepes-NaOH, pH 7.3, 10 mM MgCl$_2$, 1 mM DTT, 100 μg/ml BSA, 5% (vol/vol) glycerol, 1 mM mercaptoethylamine]. Single-molecule fluorescence experiments were performed at room temperature (≈22 °C) using a confocal microscope with alternating-laser excitation between a 532-nm (Samba, Cobolt; operated at ≈320 μW) and a 638-nm laser (Cube, Coherent; operated at ≈60 μW), as described (6, 7). Photon arrival times were recorded and processed using custom software written in LabVIEW (National Instruments), MATLAB (MathWorks, Natick), and Python (Python Software Foundation). Alternating-laser excitation (ALEX) experiments produce four photon streams (8): $F_{Dex,Dem}$, $F_{Dex,Aem}$, $F_{Aex,Dem}$, $F_{Aex,Aem}$, where $F_{Xex,Yem}$ is the photon count detected in Y-emission wavelength upon excitation with the X-excitation laser. Fluorescence bursts corresponding to diffusing molecules were identified using an algorithm (7, 9) that searches for L photons, each having M neighboring photons within a time interval of T ms. We performed our burst search using an $F_{Aex,Aem}$ threshold to find molecules with an active acceptor. Stoichiometry, S, and apparent FRET efficiency, E^*, were calculated for each burst, yielding 2D E^*-S histograms:

$$E^* = F_{Dex,Aem}/(F_{Dex,Aem} + F_{Dex,Dem}) \qquad \textbf{[S1]}$$

$$S = (F_{Dex,Aem} + F_{Dex,Dem})/(F_{Dex,Aem} + F_{Dex,Dem} + F_{Aex,Aem}) \qquad \textbf{[S2]}$$

FCS experiments were performed using continuous 532-nm excitation (150 μW). Photon arrival times in the donor and acceptor channels were correlated using a hardware correlator (Flex02-02D, Correlator.com).

Analysis of E^* histograms. Because E^* values are sensitive to instrument conditions (8, 9), every set of measurements included a binary and a ternary complex to serve as reference points. The peak positions of the open and closed complexes were obtained by iteratively fitting the E^* histograms of the binary and ternary complexes to double-Gaussian functions. Fitting the E^* histogram of the binary complex to an unconstrained double-Gaussian yielded the mean E^* of the open conformation, which was used to constrain the fitting of the ternary complex and derive the mean E^* of the closed conformation. The closed complex E^* was then used for constraining the fit of the binary complex in order to refine the E^* for the open complex. The fitting procedure was repeated until the mean E^* values differed by <0.005 in successive iterations.

Simulations of ALEX experiments. Monte Carlo simulations of diffusing molecules in confocal microscopy have been described (10, 11). We simulated molecules diffusing within an environment defined by a 3D Gaussian excitation/detection volume. For each type of molecule, we defined its concentration, diffusion coefficient, a set of rates describing the interconversion between the open and closed states, and a set of fluorophore-specific parameters (stoichiometry, molecular brightness, and interfluorophore distance). Simulations (written in C++) were done with a 1 μs time step, much faster than diffusion (occurring at the ≈3 ms timescale) and laser alternation due to ALEX (10 kHz). Results were analyzed as with the experimental data.

E^* standard deviation analysis. The standard deviation of E^* (σ_{E^*}) for each burst was calculated using a 20-photon sliding window along the photon stream due to donor excitation ($F_{\text{Dex,Dem}}+F_{\text{Dex,Aem}}$). One E^* value was computed for every 20 consecutive photons, and all E^* values within a burst were used to compute the standard deviation, σ_{E^*}. Two-dimensional histograms (Fig. 3 B and C) show the mean E^* of each burst plotted against its σ_{E^*} for all bursts from a single experiment; binning artifacts were removed by Gaussian smoothing. Because the shot-noise-limited standard deviation of E^*, $\sigma_{E^* SN}$, depends on the photon count and the value of E^* (10)

$$\sigma_{E^* SN} = \sqrt{\frac{E^*(1-E^*)}{1+F_{\text{Dex,Dem}}+F_{\text{Dex,Aem}}}} \qquad \textbf{[S3]}$$

we calculated the expected $\sigma_{E^* SN}$ values for a 20-photon window and the entire range of E^* (dotted parabolas in Fig. 3 B and C); σ_{E^*} values that exceed the shot-noise limit are diagnostic of dynamics.

In-gel FCS experiments. In-gel FCS analysis was performed as described (12). Pol I(KF) (5 nM) was loaded onto a 5% polyacryl-

amide gel (2.6% crosslinked), poured and run in 25 mM Tris, 200 mM glycine, 10 mM MgCl$_2$, 100 μg/ml BSA, 5% (vol/vol) glycerol. For the binary complex, the hairpin DNA oligonucleotide (Fig. 1C) (1 μM) was incubated with Pol I(KF) before loading. For the ternary complex, the gel was soaked in 1 mM dTTP for 1 h before loading the sample [5 nM Pol I(KF), 1 μM hairpin DNA, and 100 μM dTTP]. FRET dynamics were analyzed using the ratio of donor autocorrelation $G_{DD}(\tau)$ and donor-acceptor cross-correlation $G_{DA}(\tau)$ due to donor excitation (12, 13). The correlation curves contain a diffusion term, $Diff(\tau)$, and a term for the conformational dynamics leading to FRET fluctuations, $R_{XY}(\tau)$:

$$G_{XY}(\tau) = Diff(\tau)R_{XY}(\tau) \qquad \textbf{[S4]}$$

Taking the ratio of $G_{DD}(\tau)$ and $G_{DA}(\tau)$ removes the diffusion term; to recover the timescale of dynamics, we fit our curves to a stretched exponential function

$$\frac{G_{DD}(\tau)}{G_{DA}(\tau)} = C(1 + Ke^{-(\tau/\tau_R)^\beta}) \qquad \textbf{[S5]}$$

where C is a constant related to the concentration of doubly labeled species, K is the equilibrium constant between the two FRET states, β is the stretch parameter (ranging from 1 for one discrete energy barrier, to 0 for a continuum of equal energy barriers), and τ_R is the relaxation time for the dynamics. The mean relaxation time is obtained using

$$\langle\tau\rangle = \int_0^\infty e^{-(\frac{t}{\tau_R})^\beta} dt = \left(\frac{\tau_R}{\beta}\right)\Gamma(\beta^{-1}) \qquad \textbf{[S6]}$$

where $\Gamma(\beta^{-1})$ is the gamma function.

1. Astatke M, Grindley NDF, Joyce CM (1998) How *E. coli* DNA polymerase I (Klenow fragment) distinguishes between deoxy- and dideoxynucleotides. *J Mol Biol* 278:147–165.
2. Turner RM, Jr, Grindley NDF, Joyce CM (2003) Interaction of DNA polymerase I (Klenow fragment) with the single-stranded template beyond the site of synthesis. *Biochemistry* 42:2373–2385.
3. Joyce CM, Derbyshire V (1995) Purification of *E. coli* DNA polymerase I and Klenow fragment. *Methods Enzymol* 262:3–13.
4. Joyce CM, et al. (2008) Fingers-closing and other rapid conformational changes in DNA polymerase I (Klenow fragment) and their role in nucleotide selectivity. *Biochemistry* 47:6103–6116.
5. Johnson KA (1995) Rapid quench kinetic analysis of polymerases, adenosinetriphosphatases, and enzyme intermediates. *Methods Enzymol* 249:38–61.
6. Doose S, Heilemann M, Michalet X, Weiss S, Kapanidis AN (2007) Periodic acceptor excitation spectroscopy of single molecules. *Eur Biophys J* 36:669–674.
7. Kapanidis AN, et al. (2008) *Single-Molecule Techniques: A Laboratory Manual*, eds Selvin PR, Ha T (Cold Spring Harbor Laboratory Press, Cold Spring Harbor, NY), pp 85–119.
8. Kapanidis AN, et al. (2004) Fluorescence-aided molecule sorting: Analysis of structure and interactions by alternating-laser excitation of single molecules. *Proc Natl Acad Sci USA* 101:8936–8941.
9. Lee NK, et al. (2005) Accurate FRET measurements within single diffusing biomolecules using alternating-laser excitation. *Biophys J* 88:2939–2953.
10. Nir E, et al. (2006) Shot-noise limited single-molecule FRET histograms: Comparison between theory and experiments. *J Phys Chem B* 110:22103–22124.
11. Wohland T, Rigler R, Vogel H (2001) The standard deviation in fluorescence correlation spectroscopy. *Biophys J* 80:2987–2999.
12. Santoso Y, Kapanidis AN (2009) Probing biomolecular structures and dynamics of single molecules using in-gel alternating-laser excitation. *Anal Chem* 81:9561-9570
13. Torres T, Levitus M (2007) Measuring conformational dynamics: A new FCS-FRET approach. *J Phys Chem B* 111:7392–7400.

Fig. S1. Characterization of fluorescently labeled Pol I(KF) derivatives. (*A*) Fluorescence emission of the single-Cys Pol I(KF) mutants, K550C and L744C, derivatized with Cy3B ("G") and ATTO647N ("R"). Cy3B was excited at 555 nm, and the height of the emission peak was measured at 575 nm. ATTO647N was excited at 644 nm, and the emission peak was at 663 nm. For each protein, the bar graph compares the fluorescence emission peaks for the unliganded Pol I(KF) (0.5 μM), the binary complex with the DNA hairpin template-primer (2 μM) shown in Fig. 1*C*, and the ternary complex formed by addition of the next complementary nucleotide, dTTP (500 μM) to the binary complex. Spectra were corrected to compensate for the dilution caused by addition of substrates and the peak heights were normalized relative to the emission peak of the unliganded protein. It is evident that the binding of these substrates has very little effect on the fluorophores attached to Cys side chains at 550 or 744. (*B*) Hairpin DNA molecule, identical to that shown in Fig. 1*C*, except for a Dabcyl-dT (*D*) at the T(-8) position (shown in context of the Pol-DNA structure in Fig. 1*B*). (*C*) The positions of Cy3B and ATTO647N in doubly labeled Pol I(KF) can be assigned based on quenching by the T(-8) Dabcyl-DNA, shown in (*B*). The height of each bar represents the Cy3B or ATTO647N emission peak when the labeled protein is bound to the T(-8) Dabcyl-DNA, as a fraction of the emission of the free protein. The labeled single-Cys proteins in the first four lanes served as standards. The right panel shows data from four preparations of doubly labeled K550C,L744C Pol I(KF). The first two were labeled with Cy3B maleimide first, followed by ATTO647N maleimide; the strong quenching of the Cy3B emission indicates that a major fraction of the Cy3B is attached at Cys550. The other two samples have the opposite labeling pattern, obtained by labeling with ATTO647N maleimide before Cy3B maleimide. (*D*) Analysis of fluorophore distribution in doubly labeled K550C,L744C Pol I(KF). SDS-PAGE fractionation (10% gel) of limited chymotryptic digests of dye-labeled proteins separated peptides in the 10–40 kDa size range. Cy3B- or ATTO647N-containing peptides were detected by their fluorescence in the green and red channels, respectively, of a Fuji FLA-5100 scanner. The leftmost four lanes are digests of the single-Cys K550C or L744C proteins labeled with Cy3B ("G") or ATTO647N ("R"), which served to identify peptides diagnostic of labeling at the 550 or 744 positions. The two arrows show examples of peptides, well separated from other fluorescent bands, which were used for quantitation. (Note that the fluorophore labels cause subtle changes in peptide electrophoretic mobility.) The fluorescence of these and other peptides was quantitated in the green and red channels, and the relative molarities of Cy3B and ATTO647N in each band were calculated (results below gel). The conversion between dye molarity and fluorescence intensity in each channel was established by measuring the fluorescence signal, in both channels, of the full length band for each doubly labeled protein. The fluorescence signal was then compared with the molarity of the corresponding dye, measured spectroscopically on the undigested protein. Lanes 1 and 2 were digests of mixtures of labeled single-Cys Pol I(KF) mutants (550-Cy3B and 744-ATTO647N in lane 1; 550-ATTO647N and 744-Cy3B in lane 2), demonstrating the reliability of the quantitation strategy. Lanes 3 and 4 were digests of doubly labeled K550C,L744C Pol I(KF); lane 3 was derived from protein labeled with Cy3B first followed by ATTO647N, and lane 4 from protein labeled with the dyes in the opposite order. A simple calculation based on the results shown below the gel indicates that, in the preparation corresponding to lane 3, 99% of those molecules that carried both a donor and acceptor dye were in the orientation $G_{550}R_{744}$. Likewise, the donor–acceptor population corresponding to lane 4 was 88% $R_{550}G_{744}$ and 12% $G_{550}R_{744}$. Note that the presence of some molecules that are unlabeled at either position 550 or 744 does not alter the calculated ratio of the two doubly labeled species. (*E*) Steady-state fluorescence anisotropy values of Cy3B and ATTO647N when attached to Cys side chains at 550 or 744. The higher anisotropy values for ATTO647N at either position indicate more restricted motion of this hydrophobic fluorophore. The values obtained were unaffected by subjecting the proteins to an additional gel-filtration step, indicating the absence of free fluorophore in the labeled protein samples.

Fig. S2. Enzymatic activity of fluorescently labeled Pol I(KF) derivatives. (*A*) The rates of dNTP addition catalyzed by Pol I(KF) derivatives with Cys substitutions and fluorophore labels were measured by chemical-quench methods (4, 5). The DNA substrate consisted of the 13-mer primer, (5′)GAGTCAACAGGTC(3′), 5′-labeled with ^{32}P, annealed to the complementary 19-mer (5′)GGTAG<u>A</u>GACCTGTTGACTC(3′), where the templating base is underlined. The reaction contained 0.5 μM duplex DNA, ≈0.25 μM Pol I(KF) and 50 μM dTTP. The rate was calculated by fitting the time course of product formation to the equation for burst kinetics.(5) (*B*) Ensemble stopped-flow fluorescence of R$_{550}$G$_{744}$ Pol I(KF), using FRET between Cy3B and ATTO647N, gave a fingers-closing rate similar to that measured previously using a different fluorescent reporter (4). Cy3B was excited at 545 nm, and the fluorescence of donor and acceptor were recorded using the dual-channel mode of an Applied Photophysics SX.18MV spectrofluorometer. Donor (Cy3B) emission was measured using a 560–590 nm bandpass filter, and acceptor (ATTO647N) emission using a 645 nm long-pass filter. After mixing, the concentrations of reactants were 0.5 μM Pol I(KF), 1 μM nonextendable (dideoxy-terminated) hairpin DNA (Fig. 1*C*), and 50 μM dTTP in 50 mM Tris-HCl (pH 7.5), 1 mM EDTA, and 5 mM MgCl$_2$. The donor signal is shown in black, with the corresponding trace obtained in the absence of dTTP shown in grey. The analogous traces for the acceptor signal are in blue (dTTP) and pale blue (control). The donor signal was fitted to a double exponential and the acceptor signal to a triple exponential. In both cases, the major fluorescence change (a decrease in donor fluorescence and an increase in acceptor fluorescence) corresponded to the fastest rate and was in agreement with our previously reported fingers-closing rate. This fast step was not observed with G$_{550}$R$_{744}$ Pol I(KF). (*C*) Stopped-flow fluorescence of R$_{550}$G$_{744}$ Pol I(KF) with an extendable DNA substrate provided information on the rates of steps that occur after fingers-closing. Reaction conditions were as in (*B*), except that the hairpin DNA had a Dabcyl-dT quencher at the T(-8) position (see Fig. S1*B*) and a 3′OH. The presence of the dabcyl quencher affects the emission from the fluorophore attached to position 550, in this case ATTO647N, which was detected with excitation at 630 nm and using a 645-nm long-pass filter. The resulting trace was fitted to a triple exponential. Rate$_1$ is a low-amplitude change, probably corresponding to fingers-closing. The fluorescence increase of Rate$_2$ probably results from translocation following chemical incorporation (which increases the distance between ATTO647N and the DNA-bound quencher), rate limited by a slower step immediately preceding or following the chemical step. Rate$_3$ is most probably dissociation of the Dabcyl-DNA, which is rate limiting for subsequent fluorescence changes that should take place because the DNA is in 2-fold molar excess over the protein. The magnitudes of these reaction rates are consistent with results from our earlier studies (4). Similar rates were obtained using singly labeled 550-Cy3B or 550-ATTO647N Pol I(KF).

Fig. S3. smFRET analysis of G$_{550}$R$_{744}$ Pol I(KF). (*A–C*) The histograms show the distribution of E^* values for (*A*) unliganded G$_{550}$R$_{744}$ Pol I(KF), (*B*) the Pol-DNA binary complex, and (*C*) the Pol-DNA-dNTP ternary complex with a complementary dNTP. The hairpin DNA oligonucleotide (Fig. 1*C*) was present at 0.4 μM and dTTP at 10 μM. As in Fig. 2, the histograms illustrated here were derived from the population of molecules labeled with both donor and acceptor fluorophores. In contrast to the R$_{550}$G$_{744}$ protein discussed in the text, the opposite labeling orientation, G$_{550}$R$_{744}$, resulted in a distribution of FRET species biased toward higher E^* values in all three situations: unliganded, Pol-DNA binary complex, and correctly paired Pol-DNA-dNTP ternary complex. Vertical dashed lines represent the positions of the open and closed states for the R$_{550}$G$_{744}$ Pol I(KF) under identical measurement conditions. Similar, though less extreme, behavior was observed with a 550-Cy3B,744-Alexa647 Pol I(KF) derivative.

Fig. S4. Open and closed complexes of $R_{550}G_{744}$ Pol I(KF). (*A*) Addition of the complementary dTTP to a binary complex of $R_{550}G_{744}$ Pol I(KF) with the hairpin DNA oligonucleotide shown in Fig. 1*C* (0.4 μM) caused an increase in the mole fraction of the closed conformation. Histograms of the E^* distribution of doubly labeled molecules were derived as described in Fig. 2. The binary Pol-DNA complex and the ternary complex with 5 μM dTTP were fitted to double-Gaussian distributions using an iterative procedure (see *Methods*) to determine the mean E^* values of the open and closed complexes (marked by vertical dashed lines). The remaining histograms were fitted to double-Gaussian distributions with their mean values constrained to those of the open and closed conformations. The fraction of molecules in the open and closed conformations was determined from the areas of the Gaussian peaks. (*B*) The fraction of molecules in the closed conformation was plotted as a function of the concentration of dTTP in the Pol-DNA-dTTP mix. Fitting this plot to a hyperbolic equation gave an apparent Kd of 0.2 μM, which is lower than the 11 μM K_d measured kinetically (4) because the two experiments measure equilibria involving different numbers of elementary steps. The smFRET approach measures the equilibrium across all the steps from the binding of the dNTP up to the formation of the closed complex, whereas the kinetic experiment relates only to those steps that precede the process whose rate is measured (the fingers-closing step, in the published data). (*C*) Open and closed complexes formed on the DNA substrate shown in (*D*) were examined in an experiment analogous to that shown in Fig. 2. The DNA was present at 0.4 μM and dATP, complementary to the templating T, was added at 2 μM to form the ternary complex. The E^* histograms were fitted, and the percentages of open and closed complexes were calculated, as described in the legend to Fig. 2. (*D*) An alternative DNA substrate used in smFRET experiments, consisting of a 21-nucleotide primer, with a dideoxy (3′H) terminus, annealed to a 62-nucleotide template. The template strand also contains a biotinylated residue at the 5′ end and an amino-modified dT residue at T(-18) on the template strand (designated as X).

Fig. S5. Residuals from Gaussian fits of the E^* histograms in Fig. 2. (*A–D*) The histograms show the fitting residuals (see Fig. 2) for (*A*) the unliganded Pol I(KF) fitted to a single Gaussian distribution (unconstrained), (*B*) the unliganded Pol I(KF) fitted to a double-Gaussian distribution (mean and standard deviation values fixed to those of the open and closed conformations), (*C*) the Pol-DNA binary complex fitted to a double-Gaussian distribution (iterative fitting, see *Methods*), and (*D*) the correctly paired Pol-DNA-dNTP ternary complex fitted to a double-Gaussian distribution (iterative fitting, see *Methods*). The residuals in all panels were normalized to the total area of the corresponding E^* histograms in Fig. 2.

Fig. S6. Investigation of the dynamic behavior of unliganded Pol I(KF) using simulations of ALEX experiments. Monte Carlo simulations of diffusing molecules excited using ALEX (see *Methods*) were used to investigate the effect of interconversion rates on the E^* histogram of unliganded Pol, shown in Fig. 2A. (A) Comparison between the time traces of experimental (Fig. 2A) and simulated data (binned at 0.5 ms) showed similar features (e.g., the levels of fluorophore brightness, molecule concentration, background level, and FRET efficiency). Three photon streams (all representing fluorescence photon counts per 0.5-ms time bin) are shown: $F_{Dex,Dem}$ is the photon count detected at the donor emission range due to excitation by the green laser; $F_{Dex,Aem}$ is the photon count detected at the acceptor emission range due to excitation by the green laser; and $F_{Aex,Aem}$ is the photon count detected at the acceptor emission range due to excitation by the red laser (see *Methods*). (B) E^* histograms obtained from simulations of molecules interconverting between the open ($E^* = 0.5$) and closed ($E^* = 0.7$) states with varying rates (forward, k_1, and backward, k_{-1}, rates were set to be equal). Simulated fluorescence-intensity timetraces were analyzed by the same procedure used for timetraces of experimental data to generate E^* histograms for diffusing molecules with one donor and one acceptor. Interconversions much faster than the diffusion time (3 ms, as measured using FCS) resulted in a single narrow peak centered between the two states. By contrast, interconversions much slower than the diffusion time appeared in the E^* histogram as two well-separated peaks centered on the individual states. Only interconversions occurring at a rate close to the time scale of diffusion generated the flat broad E^* distribution seen in the actual experimental data.

Fig. S7. Timetraces of long fluorescence bursts for Pol I(KF), its complexes, and a static-DNA control. (*A*) Representative timetraces of long fluorescence bursts (≥8 ms; burst selection was based on $F_{Aex,Aem}$ photons, using $L = 12$, $M = 6$, $T = 1$ ms; see *Methods*) generated by diffusing molecules of a static DNA control. The top panel shows photon counts upon donor excitation in the donor (green) and acceptor (red) emission channels, as well as photon counts upon acceptor excitation in the acceptor emission channel (gray), all partitioned in 0.5-ms time bins. The middle panel shows the corresponding E^* traces which demonstrate fluctuations that do not significantly exceed the shot-noise-limited standard deviation of E^*; shaded areas represent widths of $\pm 1 \sigma_{E^* SN}$. The bottom panel shows corresponding S traces; the traces are devoid of significant fluctuations, indicating that they correspond to molecules possessing active donor and acceptor fluorophores throughout their transit through the confocal volume. (*Right*) E^* and S histograms (using 0.5-ms bins) for the bursts shown. (*B*–*D*). As in (*A*), but for (*B*) unliganded $R_{550}G_{744}$ Pol I(KF), (*C*) the Pol-DNA binary complex, and (*D*) the Pol-DNA-dNTP ternary complex. Whereas the E^* traces

for unliganded Pol I(KF) demonstrate fluctuations that significantly exceed the shot-noise-limited standard deviation of E^*, the binary and ternary complexes occupy primarily the open (green shot-noise envelope) and closed (blue envelope) states, respectively, with occasional excursions to the less populated state. In the case of unliganded Pol I(KF), some examples of donor–acceptor signal anticorrelation due to FRET changes can be observed (see timetrace segments in dashed rectangles, *B*), but anticorrelation is much less apparent than in experiments using immobilized molecules because the signal is dominated by fully correlated fluorescence-intensity changes due to diffusion; the effect of diffusion can be observed in timetraces of acceptor photon counts upon acceptor excitation (gray trace, *Top*), because this photon count is not affected by FRET.
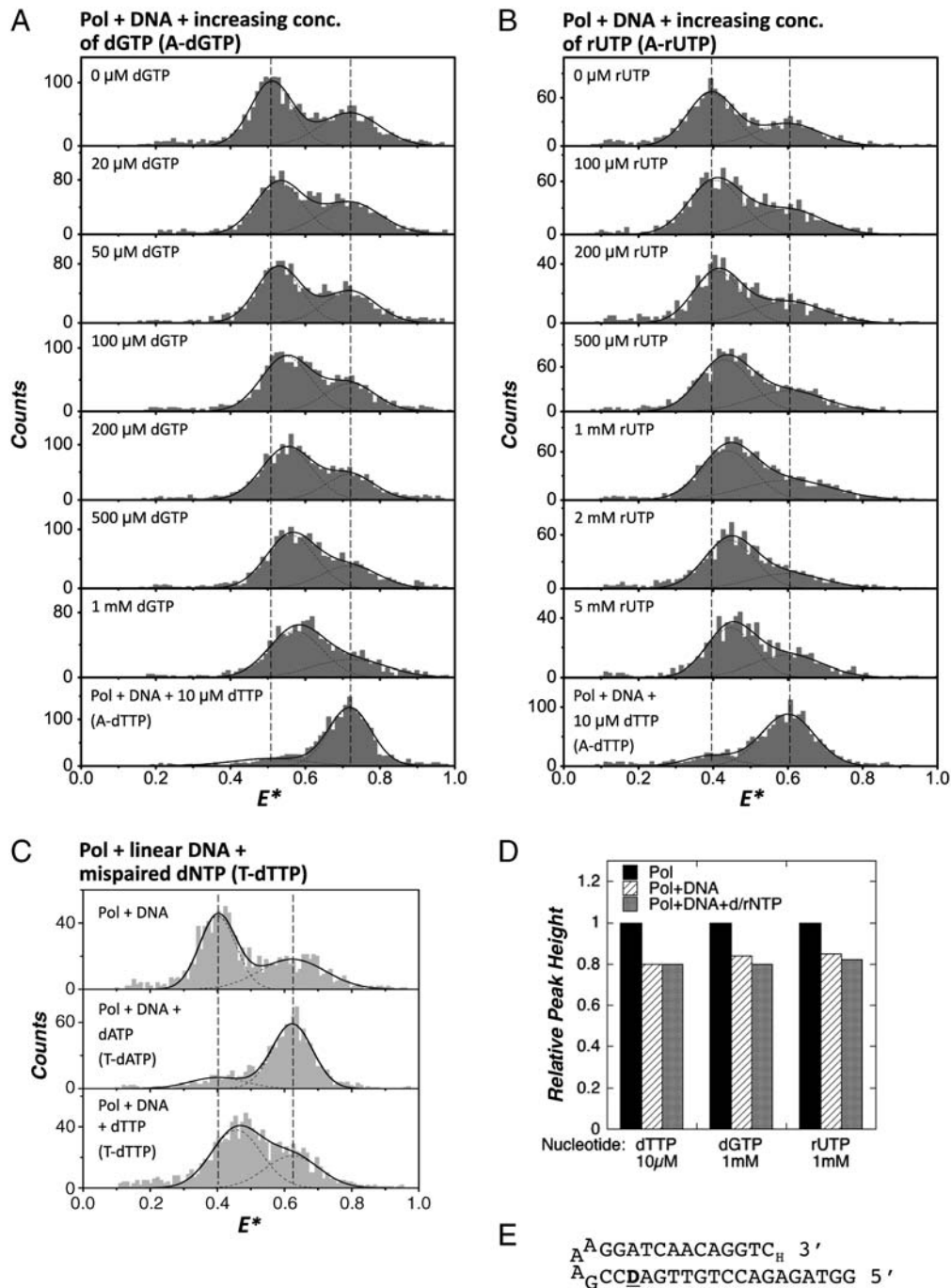
Fig. S8. Mispair and ribonucleotide complexes of $R_{550}G_{744}$ Pol I(KF). (*A*) E^* histograms of the population of doubly labeled complexes resulting from the addition of dGTP to the Pol-DNA binary complex, forming an A-dGTP mispair. The hairpin DNA (Fig. 1*C*) was present at 100 nM and dGTP was added to give the series of concentrations indicated. The two vertical dashed lines represent the mean E^* values of the open and closed conformations obtained in the same set of experiments. Each E^* histogram was fitted with two Gaussians (black solid lines, sum of Gaussians; dashed lines, individual Gaussians), with one Gaussian constrained to the mean E^* of the closed state and the other unconstrained. The shift of the mean of the lower-E^* peak was normalized relative to the E^* difference between the open and closed conformations and plotted as a function of dGTP concentration in Fig. 4*D*. Because the closed and open states are in equilibrium, the fraction of molecules in the closed conformation decreases with increasing concentration of dGTP due to their conversion into the state with lower E^*. (*B*) An experiment analogous to (*A*), except that the addition of UTP, forming a complementary A-rUTP pair, was analyzed. (*C*) An experiment analogous to that shown in Fig. 4*A*, demonstrating that a T-dTTP mispair gives a FRET species similar to that obtained with an A-dGTP mispair (causing the E^* of the lower-E^* population to shift by ≈25% of the ΔE^* between the open and closed states). The linear dideoxy-terminated DNA duplex (Fig. S4*D*) was present at

100 nM and dTTP at 1 mM. The mean E^* values for the open and closed complexes (marked by vertical dashed lines) were obtained using the same DNA duplex, in the presence and absence of 10 μM dATP, under identical conditions. Gaussian fits of the E^* histograms were carried out as described in Fig. 4*A* (black solid lines, sum of Gaussians; dashed lines, individual Gaussians). (*D*) Ensemble fluorescence measurements using singly labeled 550-Cy3B Pol I(KF) established that the addition of a mispaired dNTP or a complementary rNTP did not disrupt Pol-DNA binding. Emission spectra, with excitation of Cy3B at 510 nm, were recorded for 550-Cy3B Pol I(KF) (1 nM) alone and in the presence of a dideoxy-terminated hairpin DNA duplex (100 nM) having a Dabcyl quencher at the T(-11) position [see (*E*)]. The experiment was carried out in 50 mM Tris-HCl (pH 7.5), 1 mM EDTA, 10 mM $MgCl_2$ and 0.1 mg/ml BSA. The spectra were corrected to compensate for the dilution caused by the addition of substrates, and the peak heights (at 575 nm), relative to the emission peak of the unbound protein, were plotted as a bar graph. The dabcyl quencher causes a decrease in Cy3B fluorescence upon Pol-DNA binding. Neither the complementary dTTP (10 μM), the mispaired dGTP (1 mM), nor the complementary rUTP (1 mM) caused a significant FRET change when added to the Pol-DNA complex. In particular, dGTP or rUTP addition did not result in an increase in Cy3B fluorescence, as would be expected if DNA dissociation occurred. (*E*) Hairpin DNA molecule, similar to that shown in Fig. 1*C*, with a Dabcyl-dT (D) at the T(-11) position.